



PCCP

**Mechanism and Kinetics for both Thermal and
Electrochemical Reduction of N₂ Catalysed by Ru(0001)
based on Quantum Mechanics**

Journal:	<i>Physical Chemistry Chemical Physics</i>
Manuscript ID	CP-ART-06-2019-003187.R1
Article Type:	Paper
Date Submitted by the Author:	04-Jul-2019
Complete List of Authors:	Chen, Liang-Yu; National Cheng Kung University, Department of Chemistry Kuo, Tung-Chun; National Cheng Kung University, Chemistry Hong, Zih-Siang; lawrence berkeley national laboratory, Chemistry Cheng, Mu-Jeng; lawrence berkeley national laboratory, Chemistry Goddard, William; CALTECH, Beckman Institute, Center for Materials and Molecular Simulation

SCHOLARONE™
Manuscripts

ARTICLE

Mechanism and Kinetics for both Thermal and Electrochemical Reduction of N₂ Catalysed by Ru(0001) based on Quantum Mechanics

Received 00th January 20xx,
Accepted 00th January 20xx

DOI: 10.1039/x0xx00000x

Liang-Yu Chen,^a Tung-Chun Kuo,^a Zih-Siang Hong,^a Mu-Jeng Cheng,^{*,a} and William A. Goddard FRSC^{*,b}

The conversion of N_{2(g)} to NH_{3(g)} is an important industrial process that plays a vital role in sustaining the current human population. This chemical transformation relies heavily on the Haber-Bosch process (N₂ thermal reduction, N₂TR), which requires enormous quantities of energy (2% of the world supply) and extreme conditions (200 atm and 500 °C). Alternatively, N_{2(g)} can be reduced to NH_{3(g)} through electrochemical means (N₂ER), which may be a less energy intensive and lower-capital approach since the H atoms come from H₂O not H₂. However, N₂ER efficiency is far from satisfactory. In order to provide the basis for developing a new generation of energy efficient processes, we report the detailed atomistic mechanism and kinetics for N₂ER on Ru(0001) along with a comparison to N₂TR. We obtained these results using a new electrochemical model for quantum mechanics (QM) calculations to obtain free energy surfaces for all plausible reaction pathways for N₂ER under a constant electrode potential of 0.0 V_{SHE}. For both processes, the elementary steps involve several steps of breaking of the NN bonds, hydrogenation of surface N₂H_x or NH_x, and NH₃ release. We find similar energetics for the NN cleavage steps for both systems. However, the hydrogenation steps are very different, leading to much lower free energy barriers for N₂ER compared to N₂TR. Thus, N₂ER favors an associative route where successive hydrogen atoms are added to N₂ prior to breaking the NN bonds rather than the dissociative route preferred by N₂TR, where the NN bonds are broken first followed by the addition of Hs. Our QM results provide the detailed free energy surfaces for N₂ER and N₂TR, suggesting a strategy for improving the efficiency of N₂ER.

Introduction

Ammonia (NH₃) is an essential chemical that plays a key role in the formation of nitrates required for fertilizer production to sustain a growing human population.¹ NH₃ could also be used as a potential substitute for traditional fossil fuels due to its carbon-free and high-energy density² and H₂ storage in fuel cell applications.^{3, 4} Currently, most ammonia is produced through the Haber-Bosch (HB) process (N_{2(g)} + H_{2(g)} → NH_{3(g)}, N₂ thermal reduction, N₂TR), which requires the reaction to proceed at high temperatures (400 - 500 °C) and high pressures (100 - 200 atm).

The HB process is energy intensive (consuming 2% of the world supply of energy) and relies heavily on fossil fuel as the energy source and chemical feedstock.⁵ The H₂ required for the process is produced through steam reforming of methane, leading to the release of huge quantities of CO₂, a greenhouse gas. In fact, ammonia production is responsible for 0.5% of global

CO₂ emissions.⁵ Moreover, to attain sufficient activity, high temperatures are required despite the exergonic nature of the process. This then requires high pressures to shift the equilibrium toward NH₃ formation, leading to very significant increases in capital costs.

An alternative approach to reduce N₂ to NH₃ involves N₂ electrochemical reduction (N₂ER) where the hydrogen for the reduction is obtained from water rather than H_{2(g)}. In addition, the required electricity could be obtained from renewable energy sources. The advantages of N₂ER are as follows:

- The thermodynamic equilibrium can be shifted toward the product side by adjusting the electrode potential.
- The reaction can proceed at ambient pressures and temperatures, reducing the capital costs for NH₃ production.

However, production of NH₃ via N₂ER is currently very inefficient with Faradaic efficiencies less than 12% and most of the consumed electricity is wasted in the hydrogen evolution reaction (HER).⁶⁻⁹ To make N₂ER commercially accessible, new strategies are needed to improve the efficiency.

As a first step toward making N₂ER commercially accessible, we developed a detailed mechanistic study considering both the thermodynamics and kinetics for all steps in the reduction of N₂ to NH₃. We consider ruthenium since it is a catalyst for both N₂TR and N₂ER. This reduction is very efficient for N₂TR¹⁰ but not for N₂ER.⁶ We used quantum

^a Department of Chemistry, National Cheng Kung University, Tainan, Taiwan. Email: mjcheng@mail.ncku.edu.tw

^b Materials and Process Simulation Center (139-74), California Institute of Technology, Pasadena, California 91125, United States. Email: wag@caltech.edu. Electronic Supplementary Information (ESI) available: Optimized coordinates for each stationary state in the N₂TR and N₂ER are provided. See DOI: 10.1039/x0xx00000x

mechanics (QM) calculations to determine the reaction mechanism for N₂TR and N₂ER catalysed by Ru(0001).

Computational Details

The PBE functional¹¹ combined with projector augmented wave pseudopotentials^{12, 13} (400 eV energy cutoff) as implemented in the Vienna ab initio Simulation Package (VASP)¹⁴⁻¹⁷ was used to perform the calculations on both the slab and molecular systems. To accelerate SCF convergence, we adopted a Gaussian-smearing technique with a smearing parameter of $k_B T = 0.1$ eV for slabs and 0.01 eV for molecules to allow fractional occupation of the one-electron energy levels. The calculated electronic energy was extrapolated to $k_B T = 0$ to obtain E_{elect} . Although spin-polarized wavefunctions were used for all slab calculations, the magnetic moment converged to zero in each case.

The Ru(0001) surface was simulated using a 3×3 three-layer slab with substrates adsorbed on the top layer. This slab model was cleaved from bulk Ru with cell parameters of $a = b = 2.700$ Å and $c = 4.275$ Å.¹⁸ During geometric optimizations, the bottom single layer was fixed in its bulk position, and the top two layers and adsorbed substrates were allowed to relax. The climbing image nudged elastic band method¹⁹ and dimer method^{20, 21} were used to locate the transition states. A Monkhorst-Pack k-point net of 3×3×1 was chosen to sample the reciprocal space for the slab calculations. Using a denser k-point net of 5×5×1 only leads to small changes in energetics (less than 0.03 eV). For the molecule calculations, only the gamma point was sampled. To prevent interactions between the periodic replicas along the z-direction in the slab calculations, a vacuum separation of at least 50 Å between adjacent images was used,²² and a 20 Å×20 Å×20 Å box was used for the isolated molecule calculations.

All energetics reported in this study are free energies. For the slab systems, we used the following equation:

$$G = E_{\text{elect}} + ZPVE + \sum_{\nu} \frac{h\nu}{e^{h\nu/k_B T} - 1} - TS_{\text{vib}}$$

For the surface adsorbates, the vibrational frequencies were evaluated using a partial Hessian matrix via the finite difference approach. Then, these frequencies were used to calculate the zero-point vibrational energy (ZPVE), thermal corrections for the enthalpies, and vibrational entropy (S_{vib}). For the free molecule systems, the free energies were estimated as follows:

$$G = E_{\text{elect}} + ZPVE + \sum_{\nu} \frac{h\nu}{e^{h\nu/k_B T} - 1} + \frac{n}{2} k_B T - T(S_{\text{trans}} + S_{\text{rot}} + S_{\text{vib}}),$$

where n is eight for non-linear molecules and seven for linear molecules. In contrast to the slab systems, the ZPVE, vibrational component of the internal energy, S_{vib} , S_{rot} , and S_{trans} were calculated at the PBE/6-311++G** level of theory using Jaguar.

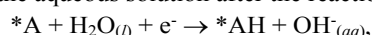
For the N₂ER, the electrochemical model proposed by Head-Gordon et al.,²³ Goddard et al.,^{24, 25} and Sautet et al.²⁶ was used to calculate the free energy surfaces under a constant electrode potential of $U = 0.0$ V_{SHE} ($U_{0,0}$), which is known as Grand Canonical QM (GC-QM). In GC-QM, the Fermi energy is adjusted to a target value by varying the number of electrons

in the system during each step in the geometry optimization, allowing us to fix the work function of the system (Φ) and thus U . The Poisson-Boltzmann implicit solvation model²⁷ was used to neutralize the non-zero charge in the simulation cell and simulate water (with a dielectric constant of 78.4). Using $\Phi_{\text{SHE}} = 4.3$ eV (the experimentally determined work function of the standard hydrogen electrode),²⁸ we calculated U as follows:

$$U = \frac{\Phi - \Phi_{\text{SHE}}}{e}$$

This model has been applied to investigate CO₂ electrochemical reduction,^{22-25, 29, 30} as well as pyridine²⁶ and N-heterocyclic carbene³¹ adsorption on Au(111).

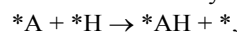
For each hydrogenation step in N₂ER, H₂O_(l) was used as the hydrogen source. We assumed that one electron is transferred into the system during the reaction while OH⁻ is formed and released into the aqueous solution after the reaction as follows:



where *A and *AH represent the adsorbed reactant and hydrogenated product, respectively. The reaction free energy is calculated as follows:

$$\Delta G = [G(*AH) + G(OH_{(aq)})] - [G(*A) + G(H_2O_{(l)}) + G(e^-)].$$

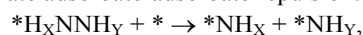
Using the definition of the standard hydrogen electrode³² and the procedure proposed by Xiao et al.,³³ $G(H_2O_{(l)}) + G(e^-) - G(OH_{(aq)})$ is equal to $\frac{1}{2}G(H_{2(g)})$ at $U_{0,0}$ and pH = 0.0, leading to $\Delta G = G(*AH) - G(*A) - \frac{1}{2}G(H_{2(g)})$. For the hydrogenation steps in N₂TR, adsorbed hydride is used as the hydrogen source:



where *H and * represent a surface-bound hydride and a clean surface, respectively. The reaction free energy is calculated as follows:

$$\Delta G = [G(*AH) + G(*)] - [G(*A) + G(*H)].$$

For the NN cleavage steps in both N₂TR and N₂ER, the reaction free energy was calculated by assuming that when NN cleavage is complete, the two newly formed species migrate far from each other to eliminate adsorbate-adsorbate repulsion:



where *H_XNNH_Y, *NH_X, and *NH_Y are surface-bound H_XNNH_Y, NH_X, and NH_Y, respectively. Thus, the reaction free energy is calculated as follows:

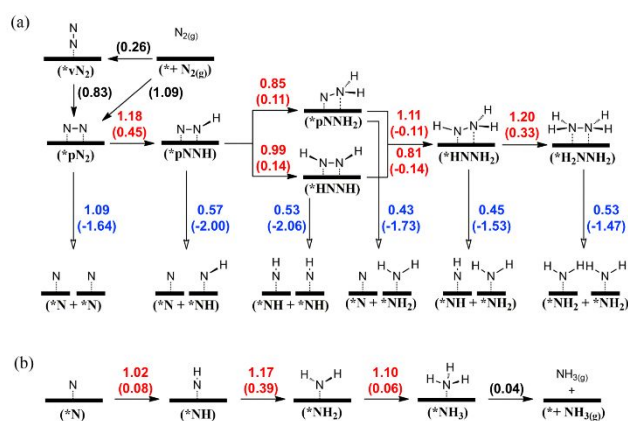
$$\Delta G = [G(*NH_X) + G(*NH_Y)] - [G(*H_XNNH_Y) + G(*)].$$

Results and Discussion

Reaction Mechanisms for N₂ Thermal Reduction on Ru(0001)

First, the N₂ thermal reduction (N₂TR, N_{2(g)} + H_{2(g)} → NH_{3(g)}) was investigated. The free energy surface was constructed at 700 K and 100 atm because the reaction often proceeds at high temperatures (400 ~ 500 °C) and pressures (100 ~ 150 bar).³⁴ Dissociative adsorption of H_{2(g)} to form surface-bound hydride (*H) on Ru(0001) is thermodynamically downhill at 700 K and 100 atm ($* + \frac{1}{2} H_{2(g)} \rightarrow *H$, $\Delta G = -0.18$ eV, the coverage is 1/9 for *H). Therefore, we assumed that sufficient *Hs on the surface are available for nitrogen reduction. This ΔG also suggests that the reverse reaction is unlikely in the N₂TR.

In this study, Ru(0001) was chosen to catalyze N_2 reduction due to its surface energy being lower than those of other low index surfaces.³⁵ To be reduced, $N_{2(g)}$ must be in contact with the catalyst, and thus, the first step involves adsorption of $N_{2(g)}$ on Ru(0001). $N_{2(g)}$ was able to adsorb on the surface in either a vertical ($*vN_2$) or parallel ($*pN_2$) configuration, which is consistent with previous theoretical results.³⁶⁻⁴⁰ The adsorption free energies were 0.26 eV for $*vN_2$ and 1.09 eV for $*pN_2$ (Scheme 1) with the vertical mode being more stable. The predicted preferred adsorption mode is also consistent with the results from previous studies.^{36, 37} Adsorbed N_2 can be hydrogenated to form $*NNH$ or undergo NN cleavage to form two $*Ns$. For the hydrogenation pathway ($*pN_2 \rightarrow *pNNH$), the free energy barrier is $\Delta G^\ddagger = 1.18$ eV, and the reaction free energy is $\Delta G = 0.45$ eV. For the cleavage pathway ($*pN_2 \rightarrow *N + *N$), the free energy barrier is $\Delta G^\ddagger = 1.09$ eV with a reaction free energy of $\Delta G = -1.64$ eV. Thus, NN cleavage is slightly more favorable by a factor of 4.45 at 700 K based on transition state theory. Attempts to locate the transition state for $*vN_2 \rightarrow *vNNH$ failed, leading to the conclusion that this hydrogenation route is not accessible.



Scheme 1. Schematic description of possible elementary steps for the N_2 TR. The numbers in parentheses are ΔG_s , and the number without parentheses are ΔG^\ddagger_s . The unit is eV.

Most previous theoretical studies on Ru³⁷ assumed that N_2 TR followed a dissociative mechanism in which $*pN_2$ is dissociated to $*N + *N$ at the very beginning of the reaction. Therefore, studies of the hydrogenation of the dinitrogen intermediates (e.g., $*pN_2$, $*pNNH$, and $*HNNH$) are limited with only two reports investigating hydrogenation.^{41, 42} One study only reported the thermodynamics and ignored the kinetics,⁴² and the other report focused on the Ru(0001) stepped surface rather than the terraced surface and investigated only the first hydrogenation reaction of $*pN_2$.⁴¹ Thus, our current study of the free energies considering thermodynamics and kinetics for both NN cleavage and hydrogenation of all dinitrogen intermediates is the first report to provide a complete picture of N_2 TR on Ru(0001).

Hydrogenation of the newly formed $*pNNH$ can lead to either $*pNNH_2$ or $*HNNH$. The energetics are as follows:

- $\Delta G^\ddagger/\Delta G = 0.85/0.11$ eV for $*pNNH \rightarrow *pNNH_2$.
- $\Delta G^\ddagger/\Delta G = 0.99/0.14$ eV for $*pNNH \rightarrow *HNNH$

Both the kinetics and thermodynamics slightly favor the formation of $*pNNH_2$. Alternatively, $*pNNH$ can proceed via NN cleavage pathway with the following energetics:

- $\Delta G^\ddagger/\Delta G = 0.57/-2.00$ eV for $*pNNH \rightarrow *N + *NH$ compared to
- $\Delta G^\ddagger/\Delta G = 1.09/-1.64$ eV for $*pN_2 \rightarrow 2* N$.

Therefore, the addition of one hydrogen to $*N_2$ dramatically reduces ΔG^\ddagger for NN cleavage by $\sim 50\%$, leading to a far more facile cleavage reaction. This result is not surprising because binding with hydrogen decreases the NN bond order and thus its bond strength ($R_{N-N} = 1.34$ Å in $*pNNH$, $R_{N-N} = 1.21$ Å in $*pN_2$). Overall, this 1-H reduction intermediate ($*pNNH$) favors NN cleavage over hydrogenation, which is similar to the situation for $*pN_2$.

In the next step, these two 2-H reduction intermediates can be either hydrogenated or NN cleaved. For $*pNNH_2$, the energetics are as follows:

- $\Delta G^\ddagger/\Delta G = 1.11/-0.11$ eV for $*pNNH_2 \rightarrow *HNNH_2$
- $\Delta G^\ddagger/\Delta G = 0.43/-1.73$ eV for $*pNNH_2 \rightarrow *N + *NH_2$.

For $*HNNH$, the energetics are as follows:

- $\Delta G^\ddagger/\Delta G = 0.81/-0.14$ eV for $*HNNH \rightarrow *HNNH_2$
- $\Delta G^\ddagger/\Delta G = 0.53/-2.06$ eV for $*HNNH \rightarrow *NH + *NH$.

Our analysis of the two types of elementary reactions for the two 2-H reduction intermediates indicates that NN cleavage remains much more favorable than hydrogenation. The search for a transition state for $*pNNH_2 \rightarrow *N + *NH_3$, where hydrogenation leads to simultaneous NN cleavage and $*NH_3$ formation, failed. In fact, no such transition state can be located for the N_2 TR.

For $*HNNH_2$, which is the common product from the $*HNNH$ and $*pNNH_2$ hydrogenation reactions, the energetics for the two types of elementary reactions are as follows:

- $\Delta G^\ddagger/\Delta G = 1.20/0.33$ eV for $*HNNH_2 \rightarrow *H_2NNH_2$
- $\Delta G^\ddagger/\Delta G = 0.45/-1.53$ eV for $*HNNH_2 \rightarrow *NH + *NH_2$.

For $*HNNH_2$, NN cleavage is still more favorable than hydrogenation. Finally, for $*H_2NNH_2$, the only possible reaction is NN cleavage as follows:

$$\Delta G^\ddagger/\Delta G = 0.53/-1.47 \text{ eV for } *H_2NNH_2 \rightarrow *NH_2 + *NH_2$$

Based on analysis of the free energy surfaces for the reactions involving dinitrogen intermediates, two interesting trends were observed.

- First, the hydrogenation pathway resulting in simultaneous NN cleavage and $*NH_3$ formation (e.g., $*pNNH_2 \rightarrow *N + *NH_3$) does not exist. Therefore, $*NH_3$ cannot be generated directly from dinitrogen species.
- The second and most important trend is that for all dinitrogen intermediates, NN cleavage is more facile than the corresponding hydrogenation due to lower ΔG^\ddagger s and much more downhill ΔG s (< -1.0 eV).

Therefore, NN cleavage occurs in the very early stage of the reaction for N_2 TR, and $NH_{3(g)}$ formation follows a dissociative mechanism, which is consistent with previous experimental⁴³⁻⁴⁷ and theoretical studies.^{36-40, 48-50}

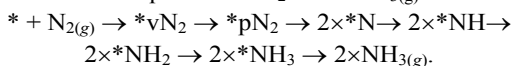
Due to the lack of a direct route for $*NH_3$ formation through the hydrogenation of dinitrogen intermediates, $*NH_3$ must be produced through hydrogenation of the mononitrogen species, which are formed from NN cleavage of dinitrogen intermediates. Therefore, we investigated the hydrogenation of the three

possible mononitrogen intermediates. The energetics are as follows:

- $\Delta G^*/\Delta G = 1.02/0.08$ eV for $*N \rightarrow *NH$
- $\Delta G^*/\Delta G = 1.17/0.39$ eV for $*NH \rightarrow *NH_2$
- $\Delta G^*/\Delta G = 1.10/0.06$ eV for $*NH_2 \rightarrow *NH_3$.

Among these three reactions, the most facile reaction is $*N \rightarrow *NH$, and the most challenging is $*NH \rightarrow *NH_2$, which is in good agreement with the previous theoretical study reported by Hu and co-workers.⁴⁸ Finally, $NH_3(g)$ is formed through molecular desorption with $\Delta G = 0.04$ eV.

Based on the calculated energetics for dinitrogen and mononitrogen intermediates, we determined that the most favorable reaction sequence for N_2TR to $NH_3(g)$ is as follows:



The ΔG for the overall reaction ($N_{2(g)} + 6 \times *H \rightarrow 2 \times NH_3(g) + 6 \times *$) is 0.59 eV, and using $H_{2(g)}$ rather than $*H$ as the reference ($N_{2(g)} + 3 \times H_{2(g)} \rightarrow 2 \times NH_3(g)$), the ΔG is -0.47 eV. These results lead to the free energy surface shown in Fig. 1. Based on this surface, the rate-determining step (RDS) is $*pN_2 \rightarrow 2 \times *N$ with an apparent kinetic barrier of 2.19 eV (referenced to $* + N_{2(g)}$), consistent with experimental results.⁵¹

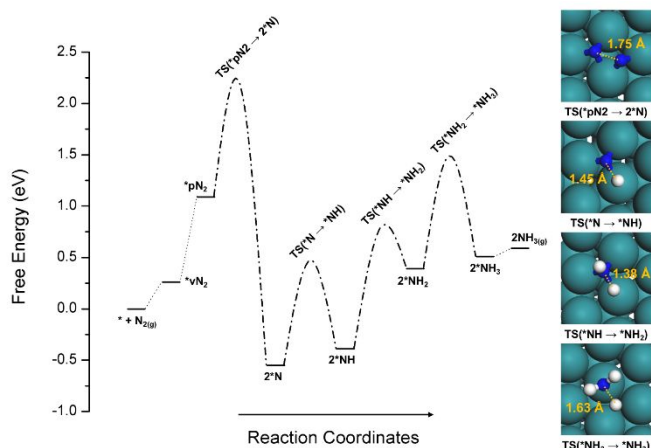


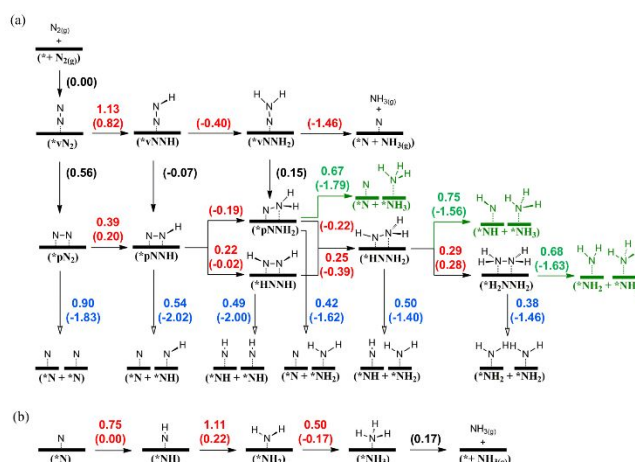
Fig. 1. Free energy surface for the most favorable reaction mechanism for N_2TR .

Reaction Mechanisms for N_2 Electrochemical Reduction on Ru(0001)

With the mechanism for the N_2TR in hand, the mechanism of N_2ER to $NH_3(g)$ on Ru(0001) under $U_{0.0}$ (aqueous phase, pH = 0.0, T = 298 K, P = 1 atm) was examined. For N_2ER , $* + N_{2(g)}$ was used as the reference to construct the free energy surfaces. The adsorption of $N_{2(g)}$ on the surface to form $*vN_2$ requires $\Delta G = 0.00$ eV, indicating that the process is thermal neutral (Scheme 2). Thus, a substantial population of $N_{2(g)}$ will be adsorbed on the surface in equilibrium. This result is similar to that reported by Skúlason et al. (i.e., $\Delta G = 0.08$ eV) for the same system.⁵² $N_{2(g)}$ can also adsorb on the surface in a parallel structure ($*pN_2$) with $\Delta G = 0.56$ eV. R_{N-N} is 1.14 Å for $*vN_2$ and 1.23 Å for $*pN_2$, suggesting that $*pN_2$ has one broken π bond.

Both $*vN_2$ and $*pN_2$ can be hydrogenated. For $*vN_2 \rightarrow *vNNH$, one additional water molecule is required to assist hydrogenation, leading to a high kinetic barrier of $\Delta G^* = 1.13$ eV

and an unfavorable $\Delta G = 0.82$ eV. Our $\Delta G = 0.82$ eV is slightly smaller than that obtained by Skúlason et al. (i.e., 1.08 eV).⁵² This discrepancy may be due to the use of the implicit solvation model and maintaining a constant electrode potential environment in our study.



Scheme 2. Schematic description of the N_2ER for each elementary step. The numbers in parentheses are ΔG s, whereas the number without parentheses are ΔG^* s. The unit is eV. The transition states for $*pNNH \rightarrow *pNNH_2$ and $*pNNH_2 \rightarrow *HNNH_2$ are lower in energy than the corresponding reactants after the ZPVE correction. Therefore, no barrier exists for these processes ($\Delta G^* = 0.00$ eV)

In contrast, for $*pN_2 \rightarrow *pNNH$, ΔG^* is 0.39, and ΔG is 0.20 eV. In reference to $*vN_2$ ($*vN_2 \rightarrow *pNNH$), ΔG^* is 0.95, and ΔG is 0.76 eV, both of which are smaller than those for $*vN_2 \rightarrow *vNNH$. Therefore, hydrogenation proceeds through $*pN_2 \rightarrow *pNNH$. More facile hydrogenation of $*pN_2$ than $*vN_2$ is not surprising because $*pN_2$ has a longer N-N bond length, indicating that one π bond was broken upon binding to the Ru surface making hydrogenation easier. This result is similar to that observed in the N_2TR catalyzed by Fe(111) system reported by us.⁵³

In addition to hydrogenation, $*pN_2$ can also proceed via NN cleavage to form $*N + *N$. $\Delta G^*/\Delta G$ was calculated to be 0.90/-1.83 eV. Because this kinetic barrier is higher than that for $*pN_2$ hydrogenation by 0.51 eV, $*pN_2$ is expected to undergo hydrogenation rather than N-N cleavage. It is important to note that for N_2ER , we determined the more favorable elementary step based on kinetics because the thermodynamics of N_2ER can become more favorable as U becomes more negative ($\Delta G(U) = \Delta G(U_{0.0}) - eU$) but the kinetics are less affected.⁵⁴

For $*pNNH$, the two possible hydrogenation pathways with the corresponding energetics are as follows:

- $\Delta G^*/\Delta G = 0.00/-0.19$ eV for $*pNNH \rightarrow *pNNH_2$
- $\Delta G^*/\Delta G = 0.22/-0.02$ eV for $*pNNH \rightarrow *HNNH$.

$*pNNH$ can also proceed via N-N cleavage with the following energetics:

- $\Delta G^*/\Delta G = 0.54/-2.02$ eV for $*pNNH \rightarrow *N + *NH$.

Based on kinetics, $*pNNH$ is expected to undergo hydrogenation rather than NN cleavage.

In the next step, both the 2-H reduction intermediates (i.e., $*pNNH_2$ and $*HNNH$) can be hydrogenated to the common intermediate (i.e., $*HNNH_2$). The energetics are as follows:

- $\Delta G^*/\Delta G = 0.00/-0.22$ for $*pNNH_2 \rightarrow *HNNH_2$
- $\Delta G^*/\Delta G = 0.25/-0.39$ eV for $*HNNH \rightarrow *HNNH_2$.

In addition, an additional hydrogenation pathway exists for $*pNNH_2$. This pathway involves hydrogen addition to the NH_2 side, leading to simultaneous $*NH_3$ formation and NN cleavage ($*pNNH_2 \rightarrow *N + *NH_3$). $\Delta G^*/\Delta G$ is $0.67/-1.79$ eV for this step, making it less favorable compared to the other processes. This direct $*NH_3$ formation pathway from the dinitrogen intermediates was not observed in N_2TR .

In addition to hydrogenation, $*pNNH_2$ and $*HNNH$ can undergo NN cleavage with the following energetics:

- $\Delta G^*/\Delta G = 0.42/-1.62$ eV for $*pNNH_2 \rightarrow *N + *NH_2$
- $\Delta G^*/\Delta G = 0.49/-2.00$ eV for $*HNNH \rightarrow *NH + *NH$.

These ΔG^* s are higher than those for the hydrogenations of $*pNNH_2$ and $*HNNH$, making NN cleavage less competitive. Because ΔG^* is 0.00 eV along the pathway, we predict that the reaction proceeds through $*pNNH \rightarrow *pNNH_2 \rightarrow *HNNH_2$.

For $*HNNH_2$, two possible hydrogenation pathways exist. The energetics are as follows:

- $\Delta G^*/\Delta G = 0.75/-1.56$ eV for $*HNNH_2 \rightarrow *NH + *NH_3$.
- $\Delta G^*/\Delta G = 0.29/0.28$ eV for $*HNNH_2 \rightarrow *H_2NNH_2$

Based on kinetics, $*HNNH_2 \rightarrow *H_2NNH_2$ is more favorable. $*HNNH_2$ can also proceed via NN cleavage with the following energetics:

- $\Delta G^*/\Delta G = 0.50/-1.40$ eV for $*HNNH_2 \rightarrow *NH + *NH_2$.

Therefore, the $*HNNH_2 \rightarrow *H_2NNH_2$ hydrogenation pathway is more favorable than NN cleavage.

Then, the newly formed $*H_2NNH_2$ can either be under hydrogenation or NN cleavage with the following energetics:

- $\Delta G^*/\Delta G = 0.68/-1.63$ eV for $*H_2NNH_2 \rightarrow *NH_2 + *NH_3$
- $\Delta G^*/\Delta G = 0.38/-1.46$ eV for $*H_2NNH_2 \rightarrow *NH_2 + *NH_2$.

Based on kinetics, we predict $*H_2NNH_2 \rightarrow *NH_2 + *NH_2$ to be more favorable.

Both direct NN cleavage and hydrogenation-induced NN cleavage generate mononitrogen species, such as $*N$, $*NH$, and $*NH_2$, on the surface. To form the target $NH_3(g)$ product and regenerate the active sites for further reactions, these species must be hydrogenated. The predicted energetics for the hydrogenation reactions as follows:

- $\Delta G^*/\Delta G = 0.75/0.00$ eV for $*N \rightarrow *NH$
- $\Delta G^*/\Delta G = 1.11/0.22$ eV for $*NH \rightarrow *NH_2$
- $\Delta G^*/\Delta G = 0.50/-0.17$ eV for $*NH_2 \rightarrow *NH_3$.

Therefore, $*NH \rightarrow *NH_2$ has the highest kinetic barrier, which should be avoided when constructing a kinetically favorable reaction sequence. $NH_3(g)$ is formed after molecular desorption with $\Delta G = 0.17$ eV.

Based on the calculated energetics and to avoid $*NH \rightarrow *NH_2$ due to its high kinetic barrier ($\Delta G^* = 1.11$), we predict that the most favorable mechanism involves $* + N_{2(g)} \rightarrow *vN_2 \rightarrow *pN_2 \rightarrow *pNNH \rightarrow *pNNH_2 \rightarrow *HNNH_2 \rightarrow *H_2NNH_2 \rightarrow 2 \times *NH_2 \rightarrow 2 \times *NH_3 \rightarrow 2 \times NH_3(g)$ (Fig. 2). Therefore, for N_2ER , facile hydrogenation leads to a mechanism following the associative route where NN cleavage occurs in the final stage after full N_2 hydrogenation. The overall ΔG ($N_{2(g)} + 6 \times (H^+ + e^-) \rightarrow 2 \times NH_3(g)$) is -0.83 eV under $U = 0.0$ V_{SHE} and pH = 0.0. This result is equivalent to $\Delta G = -0.83$ eV for $N_{2(g)} + 3 \times H_{2(g)} \rightarrow$

$2 \times NH_3(g)$ at 298 K and 1 atm based on the definition of the standard hydrogen electrode.

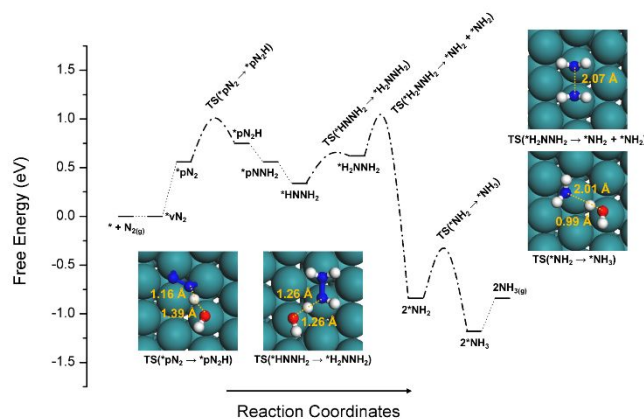


Fig 2. Free energy surface for the most favorable mechanism of N_2ER .

In reference to $* + N_{2(g)}$, we determined that $*pN_2 \rightarrow *pNNH$ (0.95 eV) and $*H_2NNH_2 \rightarrow 2 \times *NH_2$ (1.01 eV) have similar kinetic barriers. However, the high kinetic barrier of the latter is due to the free energy cost to form $*H_2NNH_2$ ($\Delta G = 0.63$ eV, $* + N_{2(g)} \rightarrow *H_2NNH_2$), which we expect to be reduced as U becomes more negative than 0.0 V_{SHE}. Therefore, each hydrogenation step would be more exothermic. Indeed, with $U_{0.5}$, $* + N_{2(g)} \rightarrow *H_2NNH_2$ is downhill by 0.95 eV (Fig. 3). Thus, we consider the RDS to be $*pN_2 \rightarrow *pNNH$ with an apparent kinetic barrier of 0.95 eV, where the adsorption of $N_{2(g)}$ to form $*pN_2$ contributes 0.56 eV and the hydrogenation of $*pN_2$ to $*pNNH$ contributes 0.39 eV.

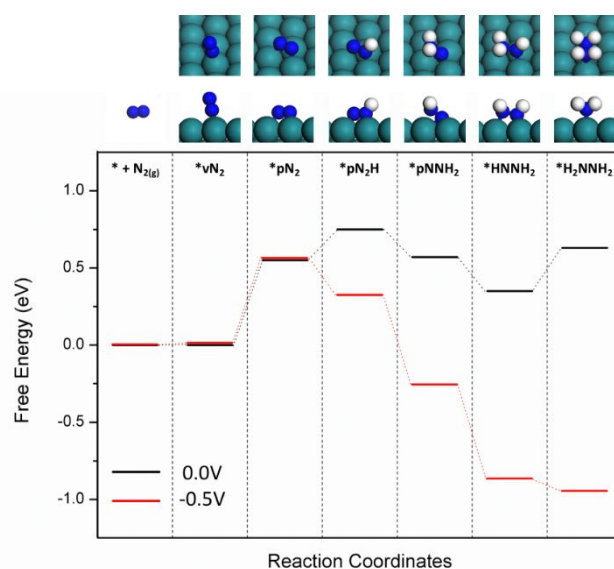


Fig 3. Free energy surfaces of N_2ER in the early stage calculated under $U_{0,0}$ (black line) and $U_{0,5}$ (red line). The unit for energy is eV.

During electrolysis, the HER competes with N_2ER for the input electricity. Based on experimental observations, most of the energy is wasted in the HER rather than the desirable N_2ER . The free surface energy for the HER was calculated. The most favorable mechanism proceeds through the Volmer-Heyrovsky

route ($* \rightarrow *H \rightarrow * + H_{2(g)}$, Fig. 4) with $\Delta G^*/\Delta G = 0.67/-0.38$ eV for $* \rightarrow *H$ and $0.82/0.38$ eV for $*H \rightarrow * + H_{2(g)}$ under $U = 0.0$ V_{SHE} and pH = 0.0. The apparent free energy barrier is 0.82 eV lower than that for the N₂ER (0.95 eV), leading to a reaction rate that is 158 times faster. Thus, our QM results are qualitatively consistent with the experimental results.

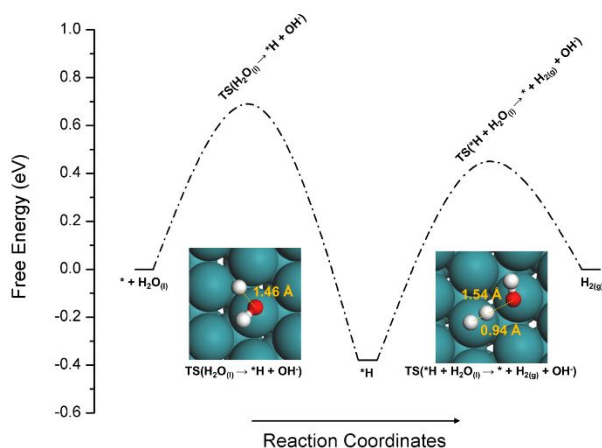


Fig 4. Free energy surface for the HER following the Volmer-Heyrovsky route.

Comparison of the N₂TR and N₂ER

By comparing the two means for N₂ reduction, we observe significant similarities and differences. The energetics for NN cleavage are similar in both reduction reactions (Table 1). The kinetic barriers values are similar with the mean absolute difference between the ΔG^* s for the two systems being only 0.08 eV. In addition, the ΔG^* s change in a similar manner. For both systems, ΔG^* decreases by ~50% after the addition of the first hydrogen. The addition of hydrogen to $*pN_2$ reduces the ΔG^* for NN cleavage from 1.09 to 0.57 eV in N₂TR and from 0.90 to 0.54 eV in N₂ER. Moreover, further addition of hydrogen only leads to a slight change in the barriers. The most significant difference between N₂TR and N₂ER is the hydrogenation step, which is much more facile in the N₂ER than in the N₂TR. On average, the ΔG^* for N₂ER is 0.66 eV smaller than that for N₂TR (Table 2). Therefore, due to the similar kinetics for NN cleavage, the more facile hydrogenation for N₂ER changes the mechanism from the dissociative route for N₂TR to the associative route for N₂ER.

Additionally, our analysis of the free energy surfaces of N₂TR and N₂ER leads to our discovery of how to improve N₂ reduction efficiency. In both systems, N_{2(g)} adsorption to form $*pN_2$ significantly contributes to the apparent kinetic barrier (i.e., 1.09 eV for N₂TR and 0.55 eV for N₂ER). As a result, the simplest method for making the processes more efficient involves reducing this adsorption energy. Because metal surface sites with low-coordinated atoms tend to bind N₂ more tightly,⁵⁵⁻⁵⁸ we expect that the use of Ru catalysts with a higher fraction of low coordinate sites will reduce N_{2(g)} more efficiently. These sites could include vacancies, steps, kinks, twins, or grain boundaries.

Table 1. Calculated ΔG^* s for N-N cleavage for N₂TR and N₂ER (unit: eV).

Reactions	N ₂ TR	N ₂ ER
$*pN_2 \rightarrow *N + *N$	1.09	0.90
$*pNNH \rightarrow *N + *NH$	0.57	0.54
$*pNNH_2 \rightarrow *N + *NH_2$	0.43	0.42
$*HNNH \rightarrow *NH + *NH$	0.53	0.49
$*HNNH_2 \rightarrow *NH + *NH_2$	0.45	0.50
$*H_2NNH_2 \rightarrow *NH_2 + *NH_2$	0.53	0.38

Table 2. Calculated ΔG^* s for hydrogenation in the N₂TR and N₂ER (unit: eV)

Reactions	N ₂ TR	N ₂ ER
$*pN_2 \rightarrow *pNNH$	1.18	0.39
$*pNNH \rightarrow *pNNH_2$	0.85	0.00
$*pNNH \rightarrow *HNNH$	0.99	0.22
$*pNNH_2 \rightarrow *HNNH_2$	1.11	0.00
$*HNNH \rightarrow *HNNH_2$	0.81	0.25
$*HNNH_2 \rightarrow *H_2NNH_2$	1.20	0.29
$*N \rightarrow *NH$	1.02	0.75
$*NH \rightarrow *NH_2$	1.17	1.11
$*NH_2 \rightarrow *NH_3$	1.10	0.50

Indeed, this strategy has been shown to work well experimentally for N₂TR. Dahl et al. demonstrated that B5 step defects on Ru(0001) are much more active than the terrace sites for NH₃ production.³⁷ We expect that this strategy would also work for N₂ER. Recent experimental studies using metallic gold with a high step density as the electrocatalyst exhibited a higher Faradaic efficiency for N₂ER,⁵⁹ supporting our hypothesis.

Additionally, our calculations showed that the formation of surface hydrogen ($*H$) is energetically favorable for both N₂TR and N₂ER:

- $\Delta G^*/\Delta G$ is 0.00/-0.36 eV for $* + H_{2(g)} \rightarrow 2*H$ for N₂TR at 700 K and 100 atm, and
- $\Delta G^*/\Delta G$ is 0.67/-0.38 eV for $* + (H^+ + e^-) \rightarrow *H$ for N₂ER under $U = 0.0$ V_{SHE} and pH = 0.

This indicates that a significant portion of the catalyst surface may be occupied by $*H$, leaving less active sites for N₂ reduction and therefore leading to a less efficient N₂ reduction process. One possible means to circumvent this problem to use proper supports such as some electride materials (e.g., Ca₂N¹⁺(e⁻) and [Ca₂₄Al₂₈O₆₄]⁴⁺(e⁻)₄)^{60, 61} and Ba-Ca(NH₂)₂,⁶² which have been shown to suppress hydrogen poisoning. Thus, ruthenium nanoparticles with higher concentrations of low coordinate sites combined with those supports may lead to more efficient NH₃ production from N₂.

Conclusion

We employed novel QM methods to predict the free energy surfaces for N₂ thermal (N₂TR) reduction and electrochemical reduction (N₂ER) on Ru(0001). Our conclusions are as follows:

- For N₂TR (at 700 K and 100 atm), N-N cleavage dominates the early stages of the reaction (the dissociation route). The most favorable reaction sequence is $* + N_{2(g)} \rightarrow *vN_2 \rightarrow *pN_2 \rightarrow 2x*N \rightarrow 2x*NH \rightarrow 2x*NH_2 \rightarrow 2x*NH_3 \rightarrow 2xNH_{3(g)}$, and the rate determining step (RDS) is $*pN_2 \rightarrow 2x*N$ with an apparent kinetic barrier of 2.19 eV (referenced to $* + N_{2(g)}$). This high kinetic barrier is due to two elementary steps including adsorption of N_{2(g)} by the surface ($* + N_{2(g)} \rightarrow *pN_2$, $\Delta G = 1.09$ eV) and the kinetic barrier required to cleave $*N_2$ to $2x*N$ ($\Delta G^* = 1.10$ eV). Therefore, improving N₂ adsorption would lead to more efficient N₂TR. This strategy has been experimentally applied to improve the performance of the N₂TR.
 - For N₂ER (at 298 K, $U = 0.0$ V_{SHE}, and pH = 0.0), hydrogenation is much more facile than NN cleavage, altering the reaction path from a dissociative route to an associative route. The reaction sequence is $* + N_{2(g)} \rightarrow *vN_2 \rightarrow *pN_2 \rightarrow *pNNH \rightarrow *pNNH_2 \rightarrow *HNNH_2 \rightarrow *H_2NNH_2 \rightarrow 2x*NH_2 \rightarrow 2x*NH_3 \rightarrow 2xNH_{3(g)}$. The RDS involves $*pN_2 \rightarrow *pNNH$ hydrogenation with an apparent barrier of 0.95 eV. This barrier is due to the adsorption of N_{2(g)} ($\Delta G = 0.56$ eV), and the kinetic barrier required for $*pN_2$ hydrogenation to $*pNNH$ is $\Delta G^* = 0.39$ eV. Thus, our results suggest that the efficiency of N₂ER can be improved by making the N_{2(g)} adsorption step less endergonic or more exergonic. This can be achieved by using ruthenium catalysts with high concentrations of undercoordinated sites.
- Conflicts of interest**
- There are no conflicts to declare.
- Acknowledgements**
- LYC, TCK, ZSH, and MJC acknowledge financial support from the Ministry of Science and Technology of the Republic of China under grant no. MOST 107-2113-M-006-008-MY2 as well as computational resource support from the National Core Facility for Biopharmaceuticals (NCFB, MOST 106-2319-B-492-002) and the National Center for High-Performance Computing (NCHC) of the National Applied Research Laboratories (NARLabs) of Taiwan. WAG acknowledges support from ONR (N00014-18-1-2155).
- Notes and references**
- J. W. Erisman, M. A. Sutton, J. Galloway, Z. Klimont and W. Winiwarter, *Nat. Geosci.*, 2008, **1**, 636-639.
 - D. W. Kang and J. H. Holbrook, *Energy. Rep.*, 2015, 164-168.
 - N. V. Rees and R. G. Compton, *Energy Environ. Sci.*, 2011, **4**, 1255-1260.
 - C. H. Christensen, T. Johannessen, R. Z. Sorensen and J. K. Norskov, *Catal. Today*, 2006, **111**, 140-144.
 - L. Wang, M. Xia, H. Wang, K. Huang, C. Qian, C. T. Maravelias and G. A. Ozin, *Joule*, 2018, 1-20.
 - V. Kordali, G. Kyriacou and C. Lambrou, *Chem. Commun.*, 2000, 1673-1674.
 - X. Ren, J. Zhao, Q. Wei, Y. Ma, H. Guo, Q. Liu, Y. Wang, G. Cui, A. M. Asiri, B. Li, B. Tang and X. Sun, *ACS Cent. Sci.*, 2018, **5**, 116-121.
 - Y. Song, D. Johnson, R. Peng, D. K. Hensley, P. V. Bonnesen, L. B. Liang, J. S. Huang, F. C. Yang, F. Zhang, R. Qiao, A. P. Baddorf, T. J. Tschaplinski, N. L. Engle, M. C. Hatzell, Z. L. Wu, D. A. Cullen, H. M. Meyer, B. G. Sumpter and A. J. Rondinone, *Sci. Adv.*, 2018, **4**, 1700336.
 - Y. Zhang, W. Qiu, Y. Ma, Y. Luo, Z. Tian, G. Cui, F. Xie, L. Chen, T. Li and X. Sun, *ACS Catal.*, 2018, **8**, 8540-8544.
 - D. E. Brown, T. Edmonds, R. W. Joyner, J. J. McCarroll and S. R. Tennison, *Catal. Lett.*, 2014, **144**, 545-552.
 - J. P. Perdew, K. Burke and M. Ernzerhof, *Phys. Rev. Lett.*, 1996, **77**, 3865-3868.
 - P. E. Blöchl, *Phys. Rev. B*, 1994, **50**, 17953-17979.
 - G. Kresse and D. Joubert, *Phys. Rev. B*, 1999, **59**, 1758-1775.
 - G. Kresse and J. Furthmüller, *Comput. Mater. Sci.*, 1996, **6**, 15-50.
 - G. Kresse and J. Furthmüller, *Phys. Rev. B*, 1996, **54**, 11169-11186.
 - G. Kresse and J. Hafner, *Physical Review B*, 1993, **47**, 558-561.
 - G. Kresse and J. Hafner, *Phys. Rev. B*, 1994, **49**, 14251-14269.
 - R. L. Clendenen and H. G. Drickamer, *J. Phys. Chem. Solids*, 1964, **25**, 865-868.
 - G. Henkelman, B. P. Uberuaga and H. Jonsson, *J. Chem. Phys.*, 2000, **113**, 9901-9904.
 - G. Henkelman and H. Jonsson, *J. Chem. Phys.*, 1999, **111**, 7010-7022.
 - P. H. Xiao, D. Sheppard, J. Rogal and G. Henkelman, *J. Chem. Phys.*, 2014, **140**.
 - H. C. Zhang, W. A. Goddard, Q. Lu and M. J. Cheng, *Phys. Chem. Chem. Phys.*, 2018, **20**, 2549-2557.
 - J. D. Goodpaster, A. T. Bell and M. Head-Gordon, *J. Phys. Chem. Lett.*, 2016, **7**, 1471-1477.
 - H. Xiao, T. Cheng and W. A. Goddard III, *J. Am. Chem. Soc.*, 2017, **139**, 130-136.
 - H. Xiao, T. Cheng, W. A. Goddard III and R. Sundararaman, *J. Am. Chem. Soc.*, 2016, **138**, 483-486.
 - S. N. Steinmann and P. Sautet, *J. Phys. Chem. C*, 2016, **120**, 5619-5623.
 - K. Mathew and R. G. Hennig, *ArXiv e-prints*, 2016, 1601.03346.
 - W. A. Donald, R. D. Leib, J. T. O'Brien, M. F. Bush and E. R. Williams, *J. Am. Chem. Soc.*, 2008, **130**, 3371-3381.
 - A. J. Garza, A. T. Bell and M. Head-Gordon, *ACS Catal.*, 2018, **8**, 1490-1499.
 - A. J. Garza, A. T. Bell and M. Head-Gordon, *J. Phys. Chem. Lett.*, 2018, **9**, 601-606.
 - K. Chang, J. G. G. Chen, Q. Lu and M. J. Cheng, *J. Phys. Chem. C*, 2017, **121**, 24618-24625.
 - J. K. Norskov, J. Rossmeisl, A. Logadottir, L. Lindqvist, J. R. Kitchin, T. Bligaard and H. Jonsson, *J. Phys. Chem. B*, 2004, **108**, 17886-17892.
 - H. Xiao, T. Cheng and W. A. Goddard, *J. Am. Chem. Soc.*, 2017, **139**, 130-136.

34. C. J. H. Jacobsen, S. Dahl, P. L. Hansen, E. Tornqvist, L. Jensen, H. Topsøe, D. V. Prip, P. B. Moenshaug and I. Chorkendorff, *J. Mol. Catal. A*, 2000, **163**, 19-26.
35. L. Vitos, A. V. Ruban, H. L. Skriver and J. Kollar, *Surf. Sci.*, 1998, **411**, 186-202.
36. J. J. Mortensen, B. Hammer and J. K. Nørskov, *Phys. Rev. Lett.*, 1998, **80**, 4333-4336.
37. S. Dahl, A. Logadottir, R. C. Egeberg, J. H. Larsen, I. Chorkendorff, E. Tornqvist and J. K. Nørskov, *Phys. Rev. Lett.*, 1999, **83**, 1814-1817.
38. A. Logadottir and J. K. Nørskov, *J. Catal.*, 2003, **220**, 273-279.
39. K. Honkala, A. Hellman, I. N. Remediakis, A. Logadottir, A. Carlsson, S. Dahl, C. H. Christensen and J. K. Nørskov, *Science*, 2005, **307**, 555-558.
40. A. Hellman, E. J. Baerends, M. Biczysko, T. Bligaard, C. H. Christensen, D. C. Clary, S. Dahl, R. van Harrevelt, K. Honkala, H. Jonsson, G. J. Kroes, M. Luppi, U. Manthe, J. K. Nørskov, R. A. Olsen, J. Rossmeisl, E. Skulason, C. S. Tautermann, A. J. C. Varandas and J. K. Vincent, *J. Phys. Chem. B*, 2006, **110**, 17719-17735.
41. A. L. Garden and E. Skulason, *J. Phys. Chem. C*, 2015, **119**, 26554-26559.
42. T. H. Rod, A. Logadottir and J. K. Nørskov, *J. Chem. Phys.*, 2000, **112**, 5343-5347.
43. L. Romm, G. Katz, R. Kosloff and M. Asscher, *J. Phys. Chem. B*, 1997, **101**, 2213-2217.
44. H. Shi, K. Jacobi and G. Ertl, *J. Chem. Phys.*, 1993, **99**, 9248-9254.
45. H. Dietrich, P. Geng, K. Jacobi and G. Ertl, *J. Chem. Phys.*, 1996, **104**, 375-381.
46. L. Diekhoner, H. Mortensen, A. Baurichter, A. C. Luntz and B. Hammer, *Phys. Rev. Lett.*, 2000, **84**, 4906-4909.
47. R. C. Egeberg, J. H. Larsen and I. Chorkendorff, *Phys. Chem. Chem. Phys.*, 2001, **3**, 2007-2011.
48. C. J. Zhang, Z. P. Liu and P. Hu, *J. Chem. Phys.*, 2001, **115**, 609-611.
49. C. J. Zhang, M. Lynch and P. Hu, *Surf. Sci.*, 2002, **496**, 221-230.
50. T. Song and P. Hu, *J. Chem. Phys.*, 2007, **127**, 154706.
51. G. Ertl, *Catal. Rev.: Sci. Eng.*, 1980, **21**, 201-223.
52. E. Skulason, T. Bligaard, S. Gudmundsdottir, F. Studt, J. Rossmeisl, F. Abild-Pedersen, T. Vegge, H. Jonsson and J. K. Nørskov, *Phys. Chem. Chem. Phys.*, 2012, **14**, 1235-1245.
53. J. Qian, Q. An, A. Fortunelli, R. J. Nielsen and W. A. Goddard, *J. Am. Chem. Soc.*, 2018, **140**, 6288-6297.
54. R. Guidelli, R. G. Compton, J. M. Feliu, E. Gileadi, J. Lipkowski, W. Schmickler and S. Trasatti, *Pure Appl. Chem.*, 2014, **86**, 245-258.
55. G. A. Morgan, D. C. Sorescu, Y. K. Kim and J. T. Yates, *Surf. Sci.*, 2007, **601**, 3533-3547.
56. C. R. Arumainayagam, C. E. Tripa, J. Z. Xu and J. T. Yates, *Surf. Sci.*, 1996, **360**, 121-127.
57. C. E. Tripa, T. S. Zubkov, J. T. Yates, M. Mavrikakis and J. K. Nørskov, *J. Chem. Phys.*, 1999, **111**, 8651-8658.
58. C. E. Tripa, T. S. Zubkov and J. T. Yates, *J. Phys. Chem. B*, 2001, **105**, 3724-3732.
59. D. Bao, Q. Zhang, F.-L. Meng, H.-X. Zhong, M.-M. Shi, Y. Zhang, J.-M. Yan, Q. Jiang and X.-B. Zhang, *Adv. Mater.*, 2017, **29**, 1604799.
60. M. Kitano, Y. Inoue, H. Ishikawa, K. Yamagata, T. Nakao, T. Tada, S. Matsuishi, T. Yokoyama, M. Hara and H. Hosono, *Chem. Sci.*, 2016, **7**, 5596-5596.
61. M. Kitano, Y. Inoue, Y. Yamazaki, F. Hayashi, S. Kanbara, S. Matsuishi, T. Yokoyama, S. W. Kim, M. Hara and H. Hosono, *Nat. Chem.*, 2012, **4**, 934-940.
62. M. Kitano, Y. Inoue, M. Sasase, K. Kishida, Y. Kobayashi, K. Nishiyama, T. Tada, S. Kawamura, T. Yokoyama, M. Hara and H. Hosono, *Angew. Chem. Int. Ed.*, 2018, **57**, 2648-2652.